March, 2002

Stress Field in Finite Width Axisymmetric Wound Rolls

Jonathan A. Wickert, *Carnegie Mellon University*
Y.M. Lee, *Carnegie Mellon University*

Stress Field in Finite Width Axisymmetric Wound Rolls

Y. M. Lee
Associate Mem. ASME

J. A. Wickert
Fellow ASME

Department of Mechanical Engineering,
Carnegie Mellon University,
Pittsburgh, PA 15213-3890

A model is developed for predicting the stress field within a wound roll of web material, in which the radial, circumferential, transverse, and shear stresses can vary in both the roll's radial and cross-web (transverse) directions. As has been the case in previous wound roll stress analyses based on one-dimensional models, the present approach accounts for the anisotropic and nonlinear material properties of the layered web material, and the incremental manner in which the roll is wound. In addition, the present development accounts for arbitrary cross-sectional geometry and material of the core, and the presence of nonuniform tension across the web's width during winding. The solution is developed through an axisymmetric, two-dimensional, finite element analysis which couples individual models of the core and layered web region substructures. The core's stiffness matrix at the core-web interface provides a mixed boundary condition for the web region's first layer. In several parameter studies, variations of the stress components in the roll's radial and cross-width directions are discussed and compared with predictions of the simpler companion one-dimensional model. The character of the stress field at the web region's free edges and along the core-web interface, and the possibility of stress concentration or singularity existing there, are also discussed. [DOI: 10.1115/1.1429934]

1 Introduction

Continuous sheets of metal, paper, polymer, and other thin materials are encountered in diverse products and industries. Such ''web'' materials are flexible mechanical structures that are transported under tension and at high speed during their production and processing. In short, wound rolls formed around a central core are common in manufacturing environments, and are generally the most economical and practical format for material storage and transportation.

The stress field within a roll develops incrementally as the first layer is wrapped onto a core, followed by the addition of many more discrete layers. The resulting stresses determine to a large extent the roll's quality, and can contribute to such failure modes as core collapse, interlayer buckling, and starring. While solutions to such problems can be engineered through empiricism and cut-and-try efforts, the roll's state of stress preferably meets certain design criteria. For instance, the circumferential stress within a web layer at a given point in the roll can be tensile or compressive, but excessive compression can lead to local buckling. Likewise, desirable radial stresses are large enough to prevent individual layers from slipping relative to one another, but not so great as to cause surface damage.

Research pertaining to the stress analysis of wound rolls has a rich history and has emphasized the development of one-dimensional models wherein the core and web are each treated as being infinitely wide. Those models account for anisotropic and nonlinear material properties, the bulk compliance of the core, and the roll's layered structure. Uniform mechanical properties and tension across the width are likewise specified, and a key assumption used in such one-dimensional models is the specification of core stiffness being uniform across the roll's width, a restriction that is re-examined here.

Altmann [1] treated each web layer as an orthotropic pseudoelastic material, and developed a linear wound roll model with solutions that could be expressed in the form of easily computed integrals. Motivated by applications in magnetic tape data storage, Tramposch [2,3] investigated the viscoelastic characteristics of polymeric substrates, and developed a linear, anisotropic, and time-dependent model to examine stress relaxation in wound rolls. Yagoda [4] demonstrated that the circumferential stress in the vicinity of the core depends strongly on its stiffness. In short, a soft core does not substantially resist the compression afforded by the web layers, in turn generating high compressive circumferential stresses near the core-web interface and facilitating defects. Connolly and Winarski [5] surveyed the Altmann and Tramposch formulations, presented parameter studies in Poisson ratio, radial modulus, winding tension, core radius and thickness, and evaluated such environmental factors as temperature and humidity.

Each of the aforementioned studies specified that the layered region in the wound roll had linear, albeit anisotropic, elastic properties. However, at the bulk level, the elastic modulus in the layered web region's radial direction is known to be a nonlinear function of the radial stress. Even for such seemingly well-understood materials as sheet steel or aluminum, the wound roll stress problem is intrinsically nonlinear, with the roll being properly viewed as a composite, anisotropic, and nonlinear structure ([6]). Hakiel [7] and Willett and Poesch [8] represented the layered region's effective bulk radial modulus as a polynomial function of the radial stress, and approached the solution through finite difference methods. Other processes that contribute to bulk material nonlinearity include air entrainment within the roll ([9,10]) and asperity compliance at the surfaces of the individual web layers.

Wound roll stress analysis is also governed by the effects of wound-in tension loss, viscoelastic response, and the finite deformation of materials that are substantially soft in the roll's radial direction. Good et al. [11] accounted for tension losses within centerwound rolls of highly compressible materials due to reduced interior radius. With corrected values for the wound-in tension, a modified and more accurate stress model was developed based on Hakiel's approach. Zabaras et al. [12] considered the deformation history of magnetic tape during winding and developed a hypoelastic finite element model which accounts for variable loading rates. Qualls and Good [13] extended previous linear analyses of viscoelastic winding mechanics by accounting for the roll's nonlinear bulk radial modulus. Benson [14] developed an alternative approach to the wound roll problem by accounting for the geo-

Contributed by the Applied Mechanics Division of THE AMERICAN SOCIETY OF MECHANICAL ENGINEERS for publication in the ASME JOURNAL OF APPLIED MECHANICS. Manuscript received by the ASME Applied Mechanics Division, Oct. 2, 2000; final revision, June 5, 2001. Associate Editor: J. R. Barber. Discussion on the paper should be addressed to the Editor, Professor Lewis T. Wheeler, Department of Mechanical Engineering, University of Houston, Houston, TX 77204-4792, and will be accepted until four months after final publication of the paper itself in the ASME JOURNAL OF APPLIED MECHANICS.

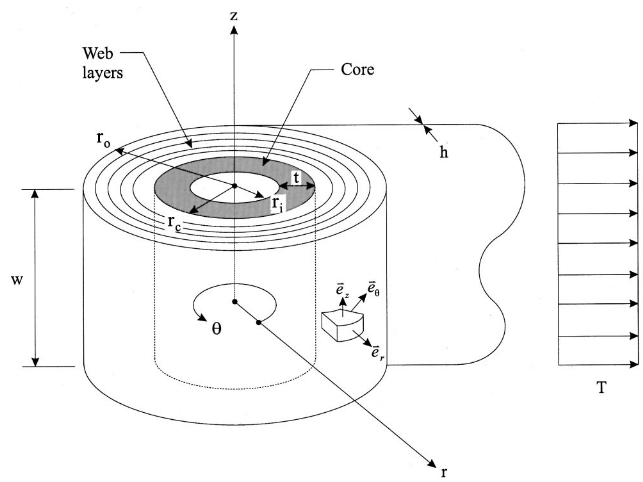

Fig. 1 Schematic of a finite width wound roll comprising the inner core and wound web regions

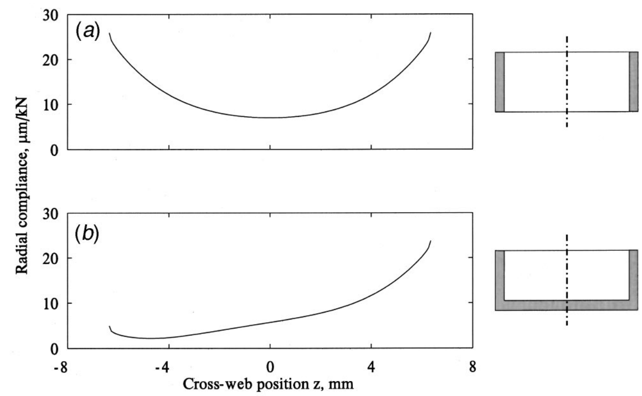

Fig. 2 Collocated point radial compliance of (*a*) hollow cylindrical and (*b*) cup-shaped cores. The parameter values are as specified in Table 1 (plastic).

metric nonlinearity that arises when web layers are highly compliant. In that approach, finite radial displacements within the roll were treated by monitoring the position of material particles using a lap index, rather than radius, so as to mark the same material location regardless of the deformation level.

These modeling issues play an important part in wound roll stress analyses, and challenge the development of efficient numerical methods to predict stresses that can vary in more than one spatial dimension. Some so-called two-dimensional wound roll models have been examined by Hakiel [15], Kedl [16], and Cole and Hakiel [17] with a view toward understanding such width-wise variations as the outside roll's radius, winding tension, and stress field due to changes in material thickness. In those views, width-wise variations were modeled under the assumptions that the roll could be partitioned across its width into strips or segments that do not couple, and that within each segment, the stresses and displacements are width-independent and can be calculated through a one-dimensional analysis.

The wound roll examined in the present study comprises core and web regions of finite width, as depicted in Fig. 1. Aside from core stiffness, the winding tension, material thickness, and elastic properties can in principle also be nonuniform. Such realistic attributes are not captured in a one-dimensional model, and it is an objective of this investigation to develop the methodology to assess their importance. To the extent that the radial compliance of the core varies along the axis of its generator, the innermost web layer is subjected to a stiffness boundary condition that varies across the web's width. In what follows, by accounting for differential core compliance, transverse stress, and shear stress, the model is capable of predicting the manner in which the wound roll's stress field varies in both the roll's radial and cross-web directions. In several parameter studies, the extent to which stresses vary in the cross-width direction is discussed, and the results are compared with those obtained from the simpler one-dimensional model. Of further interest are the character of the stress field at the web's free edges and along the core-web interface, and the possibility of stress concentration or singularity existing at those points.

2 Core and Wound Roll Model

2.1 Geometry and Boundary Conditions. Figure 1 depicts a prototypical roll of finite width w which is formed by winding continuous web material at specified tension T onto a core. Shown illustratively in Fig. 1 as a hollow cylinder, the core has inner radius r_i, wall thickness t, and coordinates $r-\theta-z$ centered in the roll. In what follows, the core is treated as having an arbitrary but axisymmetric geometry, so that the modeled problem has somewhat greater generality than that depicted in Fig. 1. The web itself has thickness h, and it is wound layer-by-layer into a cylindrical shape having outer radius r_o and inner radius r_c common with the core. As an incrementally layered structure, the web region is a composite with bulk anisotropic properties, and is formed from N individual layers that have been shrunk-fit onto one another.

The materials and elastic properties of the core and layered web regions in Fig. 1 generally differ. For two core designs, Fig. 2 depicts the manner in which the core's compliance changes in the roll's width-wise direction. Each core has properties and dimensions as specified in Table 1 (plastic). The collocated point compliance is recorded in Fig. 2 with respect to the core's radial direction. The hollow cylindrical core in Fig. 2(*a*) has a symmetric stiffness distribution in z, with the compliance at the core's free edges being some three times greater than at the centerline. For the cup-shaped core shown in Fig. 2(*b*), the asymmetric stiffness profile varies nearly tenfold between the closed and open ends. To the extent that the core's compliance establishes one boundary condition that is afforded to the layered web region, it is problem-

Table 1 Baseline parameter values used in the case studies

Core

Modulus, E	3.5 (plastic)	GPa
	70 (aluminum)	GPa
Poisson ratio, ν	0.43 (plastic)	—
	0.33 (aluminum)	—
Outer radius, r_c	25.0	mm
Width, w	12.7	mm
Thickness, t	2.5	mm

Web

Tension, T	1.0	N
Number of layers, NL	3000	—
Width, w	12.7	mm
Thickness, h	10.0	μm
Bulk modulus, E_r ($\lvert\sigma_r\rvert < 4$ MPa)	$10\lvert\sigma_r\rvert^3 - 120\lvert\sigma_r\rvert^2 + 590\lvert\sigma_r\rvert + 7$	MPa
Circumferential modulus, E_θ	7	GPa
Transverse modulus, E_z	9	GPa
Shear modulus, G_{rz}	100	MPa
Poisson ratio, $\nu_{\theta z} = \nu_{\theta r} = \nu_{zr}$	0.3	—

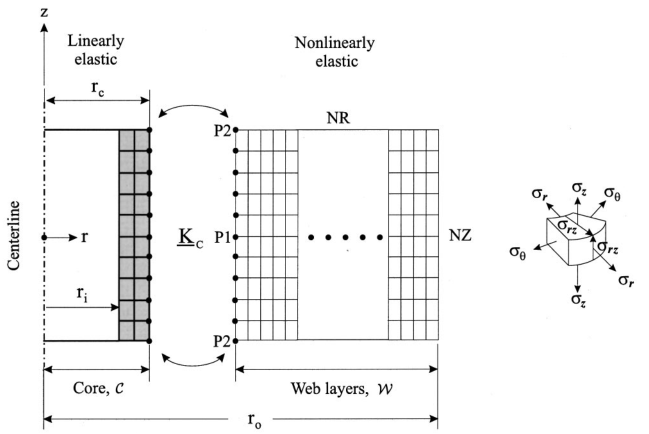

Fig. 3 Axisymmetric finite element model used to determine wound roll stresses σ_r, σ_θ, σ_z, and σ_{rz}, shown illustratively for a hollow cylindrical core

atic of one-dimensional wound roll models that such gradients and their influence on the roll's stress field cannot be captured.

Stress components σ_r, σ_θ, σ_z, and σ_{rz} within the core and web regions are each functions of r and z, and equilibrium solutions are subject to certain displacement and traction boundary conditions. For instance, rigid-body motion of a hollow cylindrical core is suppressed by specifying that transverse displacement vanishes at the center $(r_i,0)$ of the inner core's surface. As each layer is added to the roll, traction conditions over the boundary are imposed as follows:

- inner core surface $r=r_i$, $z\in[-w/2,w/2]$, and $z\neq(r_i,0)$: $\sigma_r=\sigma_{rz}=0$,
- upper and lower core surfaces $z=\pm w/2$ and $r\in[r_i,r_c]$: $\sigma_z=\sigma_{rz}=0$,
- upper and lower web surfaces $z=\pm w/2$ and $r\in[r_c,r_o]$: $\sigma_z=\sigma_{rz}=0$,
- outer web surface $r=r_o$ and $z\in[-w/2,w/2]$: $\sigma_{rz}=0$ and $\sigma_r=T/(w(r_c+(n-1)h))$

where n $(1\leqslant n\leqslant NL)$ is the integer index of the current layer, and NL is the total number of layers on the fully formed roll.

2.2 Substructure Stiffness Matrices. In order to account for realistic core geometry and designs, the wound roll is separated into substructures $\mathcal{C}=\{(r,\theta,z):r<r_c,0<\theta<2\pi,-w/2<z<w/2\}$ over the core and $\mathcal{W}=\{(r,\theta,z):r_c<r<r_o,0<\theta<2\pi,-w/2<z<w/2\}$ over the layered web region, as indicated in Fig. 3. Each substructure is discretized locally through finite element, and they couple through the interfacial core-web stiffness matrix $\boldsymbol{K}_C$. Unit loads are applied sequentially to those nodes in the core substructure's model which are located along the core-web interface, and the corresponding nodal displacements are recorded. Inversion of the flexibility matrix so obtained, formed of displacement vectors in r and z, provides matrix $\boldsymbol{K}_C$ of dimension $2(NZ+1)\times 2(NZ+1)$, where NZ is the number of elements allocated in z along the core's axis. Because of the potential variety of core materials and geometry, $\boldsymbol{K}_C$ is analyzed by using a commercial finite element package. In that manner, the present method is applicable to designs having arbitrary shape in z, and isotropic, orthotropic, or anisotropic material properties. For illustration in the case studies which follow, two prototypical core designs—cylindrical and cup-shaped—are considered, each having isotropic properties.

In terms of the layered web region, the equilibrium requirements, constitutive equations and conditions of compatibility are represented in terms of the displacement field $\boldsymbol{u}=\{uw\}^T$ as $\boldsymbol{Au}=\boldsymbol{0}$, where $\boldsymbol{A}$ is a matrix differential operator, and $u(r,z)$ and $w(r,z)$ are the radial and transverse displacements in $\mathcal{W}$, respectively. The stress field is determined through the method of weighted residuals, and the weak form of the equilibrium conditions is given by the volume integral

$$\delta\int_{\mathcal{W}}\boldsymbol{u}^T\boldsymbol{Au}\,d\mathcal{W}=0 \tag{1}$$

which provides governing equations over $\mathcal{W}$, the rectangular cross-section $\mathcal{A}=\{(r,z):r_c<r<r_o \text{ and } -w/2<z<w/2\}$, and the boundary $\delta\mathcal{A}=\{(r,z):\ r=r_c \text{ or } r=r_o \text{ and } -w/2<z<w/2\}\cup\{r_c<r<r_o \text{ and } z=\pm w/2\}$. Those conditions become

$$\int_{\mathcal{W}}\delta u\left(\frac{1}{r}(r\sigma_r)_{,r}-\frac{\sigma_\theta}{r}+\sigma_{rz,z}\right)+\delta w\left(\frac{1}{r}(r\sigma_{rz})_{,r}+\sigma_{z,z}\right)d\mathcal{W}=0 \tag{2}$$

or

$$2\pi\int_{\mathcal{A}}\delta u((r\sigma_r)_{,r}-\sigma_\theta+r\sigma_{rz,z})+\delta w((r\sigma_{rz})_{,r}+r\sigma_{z,z})d\mathcal{A}=0, \tag{3}$$

and

$$2\pi\int_{\mathcal{A}}\left(r\sigma_r(\delta u)_{,r}+r\sigma_\theta\left(\frac{\delta u}{r}\right)+r\sigma_z(\delta w)_{,z}+r\sigma_{rz}((\delta u)_{,z}+(\delta w)_{,r})\right)d\mathcal{A}-2\pi\int_{\delta\mathcal{A}}(\delta u(\sigma_r n_r+\sigma_{rz}n_z)+\delta w(\sigma_{rz}n_r+\sigma_z n_z))r\,d\delta\mathcal{A}=0, \tag{4}$$

or

$$2\pi\int_{\mathcal{A}}(\delta\boldsymbol{\epsilon}^T\boldsymbol{\sigma})r\,d\mathcal{A}-2\pi\int_{\delta\mathcal{A}}(\delta\boldsymbol{u}^T\boldsymbol{t})r\,d\delta\mathcal{A}=0 \tag{5}$$

where $\boldsymbol{n}=\{n_r,n_z\}^T$ is the unit normal, strains $\boldsymbol{\epsilon}=\{\epsilon_r,\epsilon_\theta,\epsilon_z,\gamma_{rz}\}^T$, stresses $\boldsymbol{\sigma}=\{\sigma_r,\sigma_\theta,\sigma_z,\sigma_{rz}\}^T$, and tractions $\boldsymbol{t}=\{\sigma_r n_r+\sigma_{rz}n_z,\sigma_{rz}n_r+\sigma_z n_z\}^T$.

Equation (5) is discretized locally by using four node, rectangular, axisymmetric finite elements, each having eight degrees-of-freedom. The displacement field within each element is given by

$$\boldsymbol{u}^e=\sum_{j=1}^{4}N_j\boldsymbol{a}_j^e \tag{6}$$

in terms of shape functions $N_j=(a\pm(r-r_m))(b\pm z)/(4ab)$ and nodal displacements $a_j^e=\{u_j^e w_j^e\}^T$. Here r_m, $2a$, and $2b$ are the mean radius, width, and height of each element, respectively, as in Fig. 3. The discretized (5) then becomes

$$\sum_{i=1}^{NE}\delta\boldsymbol{u}_i^{e^T}\left(2\pi\int_{\mathcal{A}^e}\boldsymbol{B}_i^T(\boldsymbol{D}_i(\boldsymbol{B}_i\boldsymbol{a}_i^e-\boldsymbol{\epsilon}_{0i})+\boldsymbol{\sigma}_{0i})d\mathcal{A}^e-2\pi\int_{\delta\mathcal{A}^e}\boldsymbol{N}_i^T\boldsymbol{t}_i r\,d\delta\mathcal{A}^e\right)=0 \tag{7}$$

where $NE=NR\times NZ$ is the total number of elements with NR in the radial direction, $\boldsymbol{D}_i$ is the elasticity matrix, $\boldsymbol{B}_i=\{\boldsymbol{\partial}\}\{\boldsymbol{N}_i\}$ is the derivative of the strain-displacement relations with $[\boldsymbol{\partial}]=[\partial/\partial r,0;1/r,0;0,\partial/\partial z;\partial/\partial z,\partial/\partial r]$, and $\boldsymbol{\epsilon}_{0i}$ and $\boldsymbol{\sigma}_{0i}$ are the initial strain and stress in the ith element.

Since $\delta\boldsymbol{u}_i^{e^T}$ in Eq. (7) is arbitrary, solutions satisfy $\boldsymbol{K}_i^e\boldsymbol{a}_i^e=\boldsymbol{f}_i^e$ in terms of the 8×8 elemental stiffness matrix

$$K_i^e = 2\pi \int_{\mathcal{A}^e} \boldsymbol{B}_i^T \boldsymbol{D}_i \boldsymbol{B}_i d\mathcal{A}^e \tag{8}$$

and the 8×1 elemental load vector

$$\boldsymbol{f}_i^e = 2\pi \int_{\delta\mathcal{A}^e} \boldsymbol{N}_i^T \boldsymbol{t}_i r d\,\delta\mathcal{A}^e + 2\pi \int_{\mathcal{A}^e} \boldsymbol{B}_i^T \boldsymbol{D}_i \boldsymbol{\epsilon}_{0i} d\mathcal{A}^e - 2\pi \int_{\mathcal{A}^e} \boldsymbol{B}_i^T \boldsymbol{\sigma}_{0i} d\mathcal{A}^e. \tag{9}$$

As the nth layer is incrementally added to the roll, the $2(n+1)(NZ+1)\times 2(n+1)(NZ+1)$ stiffness matrix over $\mathcal{W}$ is determined through $\boldsymbol{K}_W = \Sigma_{i=1}^N \boldsymbol{K}_i^e$, prior to the specification of boundary conditions. Likewise, the $2(n+1)(NZ+1)\times 1$ vector of nodal loads becomes $\boldsymbol{F} = \Sigma_{i=1}^N \boldsymbol{f}_i^e$. Summation here indicates the assembly of elemental matrices or vectors by the addition of overlapping terms at adjoining nodes, which requires a connectivity matrix relating the local elemental nodes to the global structural ones. The procedure is described in detail by Zienkiewicz and Taylor [18]. The structure-level stiffness matrix of the entire wound roll $\mathcal{R}$ having boundary conditions as specified above becomes $\boldsymbol{K}_R = \boldsymbol{K}_C + \boldsymbol{K}_W$, where assembly of the matrices corresponding to the interfacial nodes along $r = r_c$ is implied.

In this manner, the equilibrium conditions are expressed by the system of simultaneous nonlinear algebraic equations $\boldsymbol{K}_R(\boldsymbol{a})\boldsymbol{a} = \boldsymbol{F}$. As discussed in the following section, nonlinearity arises from the stress-dependent bulk properties in $\mathcal{W}$, namely $\boldsymbol{K}_W = \boldsymbol{K}_W(\boldsymbol{\sigma}_r)$.

2.3 Web Region Elasticity Matrix. The elasticity matrix $\boldsymbol{D}_i$ for each element i within $\mathcal{W}$ is an important aspect of the wound roll stress model. With each layer or group of layers having polar orthotropy, some ten material constants—moduli E_θ and E_z, bulk radial E_r, and bulk shear G_{rz} moduli, and Poisson ratios $\nu_{\theta z}$, $\nu_{\theta r}$, ν_{zr}, $\nu_{z\theta}$, $\nu_{r\theta}$, and ν_{rz}—are needed to specify properties in the web region. Even for typical, not to mention exotic materials, numerical values for those parameters are known with varying degrees of certainty, and it is problematic to estimate some of the parameters. For instance, the moduli E_θ and E_z, and ratios $\nu_{\theta z}$ and $\nu_{z\theta}$, can be readily measured. Since parameters $\nu_{\theta r}$ and ν_{zr} relate in-plane loads to out-of-plane displacements, they are challenging to measure for an already thin web layer. The specific $E_r(\sigma_r)$ dependence can be determined experimentally through standard compression testing of a stack of web material having representative dimensions ([6,8]). By fitting a polynomial curve, for instance, to the measured data, a functional expression for the bulk-level radial modulus can be obtained.

Accurate numerical values for ratios $\nu_{r\theta}$ and ν_{rz}, however, are generally not available. Their measurement requires the application of compressive forces across the layer's thickness dimension, with the measurement of corresponding displacements or strains in θ and z. In practice, however, such compression plate fixtures invariably restrict in-plane expansion through frictional contact. Thus, conventionally in the analysis of wound roll stresses and with an acknowledged view towards expediency, $\nu_{r\theta}$ and ν_{rz} are approximated on the basis of a material symmetry condition. Specifically, to the extent the roll deforms elastically and in a path-independent manner,

$$\nu_{r\theta} = \nu_{\theta r}\frac{E_r}{E_\theta}, \quad \nu_{rz} = \nu_{zr}\frac{E_r}{E_z}, \quad \nu_{z\theta} = \nu_{\theta z}\frac{E_z}{E_\theta}, \tag{10}$$

the latter of which can be directly measured in principle. For the sample polymeric material in Table 1, these conditions provide the approximations $\nu_{z\theta} = 0.233$, and at $\sigma_r = 1$ MPa compression, $\nu_{r\theta} = 0.021$ and $\nu_{rz} = 0.016$. However, because of interlayer slippage and other effects, real web materials and rolls exhibit some degree of asymmetry along the loading-unloading path. As a result, the condition (10) is not strictly applicable and should be viewed as a physically motivated approximation. In the authors' measurements on certain polymers, for instance, at identical values of σ_r, E_r values which differ by 50–100 percent between the loading and unloading portions of a compression test have been observed. To the extent that E_r is already typically much smaller than E_z and E_θ, the $\nu_{r\theta}$ and ν_{rz} values calculated through Eq. (10) are likewise small, and Benson [14] has suggested specifying $\nu_{r\theta} = \nu_{rz} \approx 0$. On the other hand, aside from the small differences in numerical values between application of the (questionable) material symmetry condition and the specification of (arbitrary) small values for $\nu_{r\theta}$ and ν_{rz}, application of Eq. (10) does have the pleasing attribute that mathematical symmetry of $\boldsymbol{K}_W$ is preserved. On balance, and from that standpoint of computational efficiency, the material symmetry condition is used here in determining $\nu_{r\theta}$, ν_{rz}, and $\nu_{z\theta}$, even while recognizing the limitations of that approximation.

With respect to the shear modulus, G_{rz} can in principle be determined experimentally by loading a stack of material in z under prescribed compressive stress, in conjunction with an angular distortion. The value so measured would be valid up to the point at which interlayer slippage began. Lacking such available measured data for G_{rz} in the literature, in case studies here, G_{rz} is specified to be constant (100 MPa) near the value (130 MPa) $E_r/(2(1+\nu_{rz}))$ at $\sigma_r = -1$ MPa. Subsequent parameter studies with various values of G_{rz} in the range 25∼400 MPa have demonstrated that the wound roll stresses are generally insensitive to G_{rz}, with variations less than five percent, except for σ_{rz} which varies with G_{rz} in a substantially proportional manner.

With these considerations in mind, $\boldsymbol{D}_i$ becomes

$$\boldsymbol{D}_i = C_0 \begin{bmatrix} E_r(1-E_z/E_\theta)\nu_{\theta\zeta}^2 & (E_\theta\nu_{r\theta} + E_z\nu_{rz}\nu_{\theta z}) & E_z(\nu_{r\theta}\nu_{rz}) & 0 \\ & E_\theta(1-(E_z/E_r)\nu_{rz}^2) & E_z(E_r\nu_{\theta z} + E_\theta\nu_{r\theta}\nu_{rz})/E_r & 0 \\ & & E_z(1-(E_\theta/E_r)\nu_{r\theta}^2) & 0 \\ \text{Symmetric} & & & G_{rz}/C_0 \end{bmatrix} \tag{11}$$

where

$$C_0^{-1} = 1 - 2(E_z/E_r)\nu_{r\theta}\nu_{\theta z}\nu_{rz} - \nu_{rz}^2(E_z/E_r) - \nu_{\theta z}^2(E_z/E_\theta) - \nu_{r\theta}^2(E_\theta/E_r). \tag{12}$$

2.4 Computation and Iteration. The equilibrium equations are written $g(\boldsymbol{a}) = \boldsymbol{K}_R(\boldsymbol{a})\boldsymbol{a} - \boldsymbol{F}$ in terms of the nodal displacements, and roots are found through Newton-Raphson iteration. As each layer or group of layers is added to the stratified $\mathcal{W}$, a truncated Taylor expansion is used to linearize about either an initial estimate at $n=1$ or the converged result $\boldsymbol{a}^*$ obtained from a previous iterate.

Computation begins by evaluating $\boldsymbol{K}_R$ at an initial estimate of the stress field. In the first iteration, the nodal displacements become $\boldsymbol{a}_1 = \boldsymbol{K}_R^{-1}(\boldsymbol{a}^*)\boldsymbol{F}$. The vector of imbalanced nodal loads in the second iteration becomes $\Delta\boldsymbol{f}_2 = \boldsymbol{K}_R(\boldsymbol{a}_1)\boldsymbol{a}_1 - \boldsymbol{F}$. The incremental nodal displacements $\Delta\boldsymbol{a}$ in the second iteration are $\Delta\boldsymbol{a}_2 = \boldsymbol{K}_R^{-1}(\boldsymbol{a}_1)\Delta\boldsymbol{f}_2$, and the cumulative displacements at that stage become $\boldsymbol{a}_2 = \boldsymbol{a}_1 + \Delta \boldsymbol{a}_2$. Generally, at the jth iteration, the imbalanced load, incremental displacement, and cumulative displacement fields are calculated through

$$\Delta \boldsymbol{f}_{j+1} = \boldsymbol{K}_R(\boldsymbol{a}_j)\boldsymbol{a}_j - \boldsymbol{F} \tag{13}$$

$$\Delta \boldsymbol{a}_{j+1} = \boldsymbol{K}_R^{-1}(\boldsymbol{a}_j)\Delta \boldsymbol{f}_{j+1} \tag{14}$$

$$\boldsymbol{a}_{j+1} = \boldsymbol{a}_j + \Delta \boldsymbol{a}_{j+1}. \tag{15}$$

For each system of locally linearized equilibrium conditions, a preconjugate gradient method is used to determine the $\Delta \boldsymbol{a}_j$, and convergence is identified by evaluating the norm $\eta = (\Sigma \Delta a_j^2 / \Sigma a_j^2)^{1/2}$. If η falls below a specified tolerance, say 10^{-3} as in the case studies below, iteration is terminated.

With the nodal displacements so obtained, the stresses within element i of the wound roll are incremented by

$$\Delta \boldsymbol{\sigma}_{ni} = \boldsymbol{D}_i(\boldsymbol{B}_i \boldsymbol{a}_i - \boldsymbol{\epsilon}_{0i}) + \boldsymbol{\sigma}_{0i} \tag{16}$$

as the nth layer is added. In turn, the cumulative stress

$$\boldsymbol{\sigma}_{ni} = \boldsymbol{\sigma}_{(n-1)i} + \Delta \boldsymbol{\sigma}_{ni} \tag{17}$$

is represented in terms of $\boldsymbol{\sigma}_{ni}$ and the stresses $\boldsymbol{\sigma}_{(n-1)i}$ developed by the first through $(n-1)$st layers.

3 Comparisons and Convergence

Results obtained from the present analysis are benchmarked against the one-dimensional model of Hakiel [7], which does include the effects of nonlinear radial modulus and uniform core compliance. Parameter values are as specified in Table 1, and for a hollow cylindrical core, Hakiel's "effective core modulus" was calculated through

$$E_c = \frac{E(1-(r_c - t)^2/r_c^2)}{(1+\nu)(r_c - t)^2/r_c^2 + (1-\nu)} \tag{18}$$

where E and ν are the core's modulus and Poisson ratio. Aside from discretization, in Hakiel [7] equilibrium is only approximately satisfied since E_r is calculated based on the stress state as the previous, not the current, layer was added, and is specified to be a constant as each layer is added. For slightly greater accuracy here, the modulus is calculated based on the stress state at the current iteration.

A comparison of σ_r and σ_θ for the two solutions is shown in Fig. 4, where values calculated along the roll's centerline $z=0$ are shown for the two-dimensional model ($NR=100$ and $NZ=80$). The two-dimensional model, which does not assume conditions of plane strain or neglect Poisson coupling as does the one-dimensional model, predicts larger values of the radial stress by some 15 percent, with peak values of -1.76 and -2.02 MPa for the two models, respectively. The maximum occurs in each case near $r=32$ mm. In terms of σ_θ, the two solutions are in close agreement along the centerline with maximum deviation at the core-web interface of less than ten percent.

In a one-dimensional model, no free edge exists along the core-web interface, and in particular, no free surface of dissimilar bonded materials exists, as is the case in a two-dimensional model (points P2, for instance, in Fig. 3). For linear, isotropic, homogeneous materials, such configurations are associated with stress concentration or even singularity, and the corner stress can be non-singular, or of order $\rho^{-\lambda}$, or $\log \rho$, where ρ is the radial distance from the corner and λ is an exponent, depending on material properties and the type of loading ([19]). In addition, in related problems of elastic inclusions within a half-space or infinite plate, the strength of the singularity depends on the ratios of the (differing) material properties of the inclusion and the surrounding material ([20]).

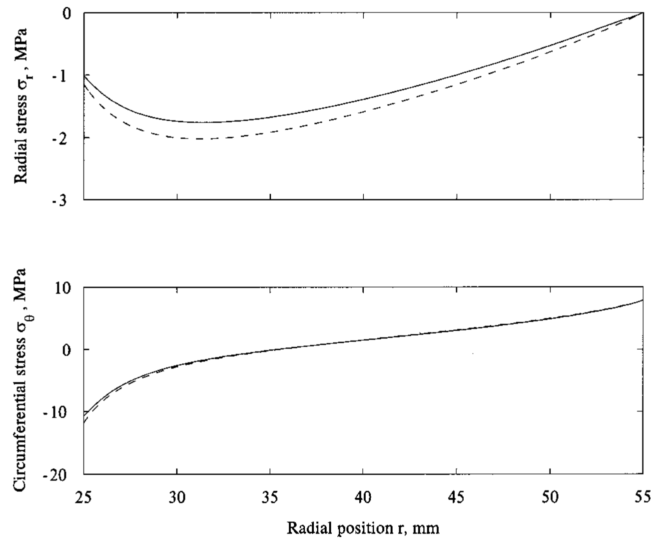

Fig. 4 Comparison of the radial and circumferential stresses along centerline $z=0$ as determined through the present (——) and one-dimensional (-----; Hakiel [7]) models. The parameter values are as specified in Table 1 (plastic, hollow core).

Dundurs [21] demonstrated that the influence of the elastic constants for two isotropic edge-bonded materials is set by the two variables $\alpha = (\bar{E}_1 - \bar{E}_2)/(\bar{E}_1 + \bar{E}_2)$ and $\beta = (\mu_1(\kappa_2 - 1) - \mu_2(\kappa_1 - 1))/(\mu_1(\kappa_2+1) + \mu_2(\kappa_1+1))$, where $\bar{E}_j = E_j$ and $k_j = (3-\nu_j)/(1+\nu_j)$ for plane stress or $\bar{E}_j = E_j/(1-\nu_j^2)$ and $\kappa_j = 3 - 4\nu_j$ for plane strain. In that formulation, E_j, ν_j, and μ_j ($j = 1,2$) are the elastic moduli, Poisson ratios, and shear moduli, of the two edge-bonded regions, and the corner stress is characterized by the numerical value of the determinant quantity $\alpha(\alpha - 2\beta)$. For strictly positive values, stresses at the corner are singular at order $\rho^{-\lambda}$; for strictly negative values, the stresses are finite and nonsingular; and for vanishing determinant, the stresses can be singular of order $\log \rho$, depending on the applied loads ([19]).

For anisotropic materials, the character of the free-edge corner stresses in ideally bonded quarter-spaces of dissimilar materials has been investigated by Wang and Choi [22,23]. That solution was developed through Lekhnitskii stress potentials, and an eigenfunction expansion was developed to obtain the stress field near the free edge. Alternative approaches have included enriched finite element and boundary integral methods which offer computational efficiency ([24]). The nature of the free-edge corner stress singularity in composite laminates remains an open issue, and the present two-dimensional model can be viewed as a tool for exploring the presence of stress concentration or singularity at the edges of the core-web interface.

With solutions here based on finite element, the presence of a singularity is only suggested by high stress gradients and/or slow convergence rates under successive mesh refinements. Such calculations identify whether stresses converge uniformly at edges of the core-web interface and enable stress concentration factors to be quantified, or whether the stresses do not converge or converge slowly, in which case singularity is possible. For properties as specified in Table 1, Fig. 5 depicts convergence of σ_r in the roll's first layer for the cases of plastic and aluminum cores. In each case, the radial stress converges quickly at point P1 ($z=0$) in Fig. 3, and for the plastic core, σ_r also converges by $NZ=40$ at points P2 ($z = \pm w/2$), namely, edges of the interface. However, with an aluminum core, the radial stress at P2 has not converged with

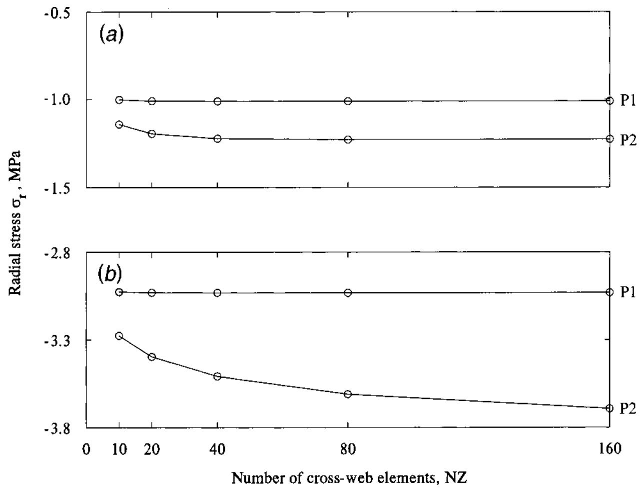

Fig. 5 Convergence of σ_r at points P1 and P2 in Fig. 3 for (*a*) plastic and (*b*) aluminum cores. The radial stress converges well along the roll's centerline in each case, and at the edge of the core-web interface for the plastic material.

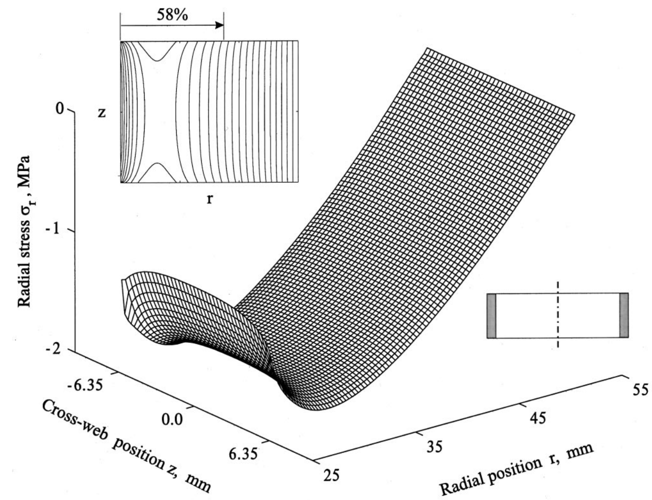

Fig. 7 Surface and contour representations of the radial and cross-web variation of σ_r; *NR*=100, *NZ*=80. The parameter values are as specified in Table 1 (plastic, hollow core).

successive mesh refinements even at $NZ=160$. This material-dependent behavior is analogous to that observed in studies of other edge-bonded regions.

When stresses are finite and converged at P2, stress concentration factors between the roll's nominal centerline stresses and those at the core-web interface's edge can be identified. The cross-web variation of σ_r in the first layer is shown in Fig. 6 for both plastic and aluminum cores. In Fig. 6(*a*) for the hollow plastic core, the stress at the edges is some $K=1.22$ times greater than the centerline value, which could be a useful quantity in analyzing wound roll defects. In Fig. 6(*b*), the shaded zones denote the regions where the stresses have not converged to three significant digits at $NZ=160$. Even in that case, however, the influence of the potential singularity is localized since the stress solution has satisfactorily converged over 90 percent of the roll's width.

4 Discussion and Further Applications

4.1 Stress Field With a Hollow Core. Figures 7–9 depict variations of the four stress components as functions of r and z for a wound roll having hollow core, dimensions, and properties as specified in Table 1. In Fig. 7, the maximum compressive radial stress of 1.89 MPa occurs at $(31.6,\pm 6.35)$ mm. The cross-width variation of σ_r diminishes with radial distance from the core. In the region $r=25\sim 30$ mm, for instance, the cross-width variation in σ_r is greater than ten percent. For the inner 58 percent of the layered region, the cross-width variation is greater than five percent but becomes smaller at larger distances from the core in accordance with St. Venant's principle.

The circumferential stress is tensile at r_o, vanishes near $r=35$ mm, and is compressive at radial locations nearer to core, and with negligible cross-width variation. In an axisymmetric structure, σ_θ depends only on radial displacement, which in turn

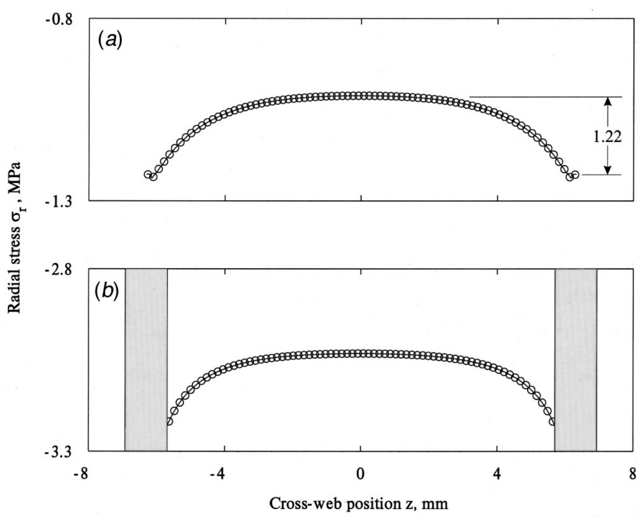

Fig. 6 Cross-web variation of σ_r along the core-web interface for hollow (*a*) plastic and (*b*) aluminum cores; *NZ*=80 (○○○○), and *NZ*=160 (——). The shaded zones in (*b*) denote regions where the stresses have not converged to three significant digits.

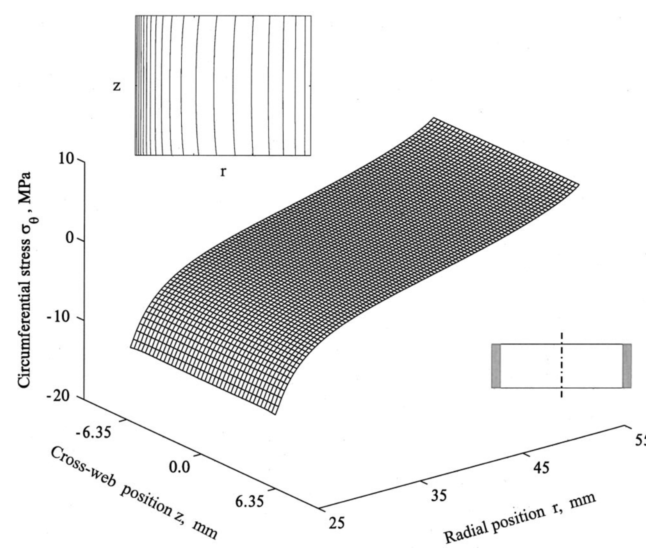

Fig. 8 Surface and contour representations of the radial and cross-web variation of σ_θ; *NR*=100, *NZ*=80. The parameter values are as specified in Table 1 (plastic, hollow core).

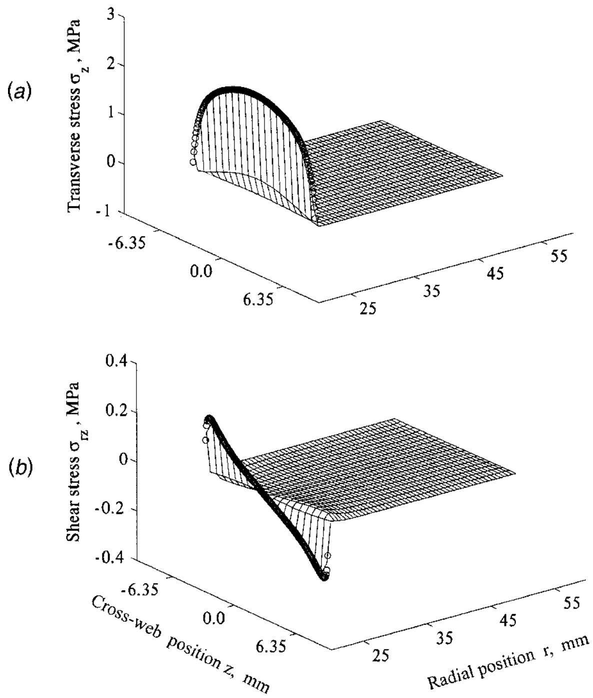

Fig. 9 Radial and cross-web variations of (*a*) σ_z and (*b*) σ_{rz}; *NZ*=80 (surface) and *NZ*=160 (○○○○; first layer only). The parameter values are as specified in Table 1 (plastic, hollow core).

is almost uniform for the chosen core design and with uniform winding tension. The maximum compressive value for σ_θ of 10.9 MPa occurs at the core-web interface.

In Fig. 9, the transverse and shear stresses are significant only near the core-web interface, and rapidly fall to almost zero elsewhere. The localized character of σ_z and σ_{rz} is attributed primarily to Poisson coupling in the core. Away from the interface, Poisson coupling is negligible because ν_{rz} and $\nu_{\theta z}$ are small, and the stresses are likewise small. Although the solutions for σ_z and

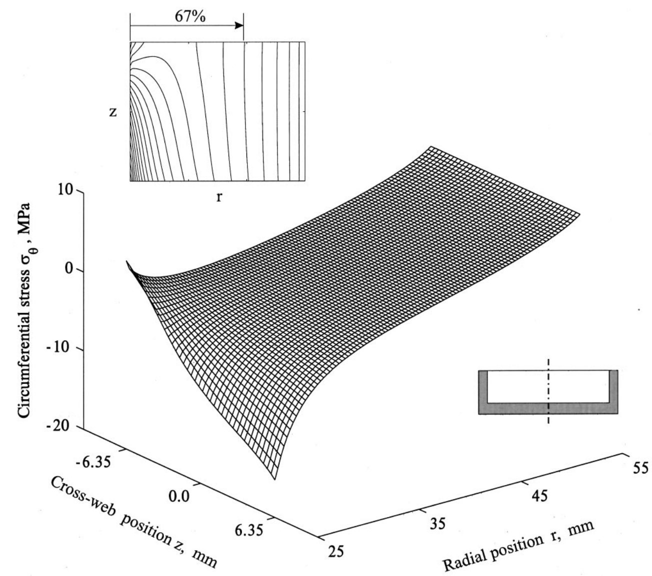

Fig. 11 Surface and contour representations of the radial and cross-web variation of σ_θ; *NR*=100, *NZ*=80. The parameter values are as specified in Table 1 (plastic, cup-shaped core).

σ_{rz} are highly localized, their solutions have converged in Fig. 9, where results for $NZ=80$ (surface) are compared in the first web layer with the results for $NZ=160$ (data points).

In the foregoing analysis, adjacent layers are assumed to remain in contact with no lateral slippage. With an assumed coefficient of friction of, say $\mu=0.3$, that assumption can be re-examined by comparing the magnitudes of σ_{rz} and $\mu\sigma_r$. Over the entire web domain, σ_{rz} is smaller, providing internal consistency at least with respect to this no-slippage assumption.

4.2 Stress Field With a Cup-Shaped Core. When the core is cup-shaped with wall thickness, width, outer radius, and plastic material properties as specified in Table 1, Figs. 10 and 11 depict the radial and circumferential stresses as functions of r and z. In the roll's first layer, the compressive radial stress varies between

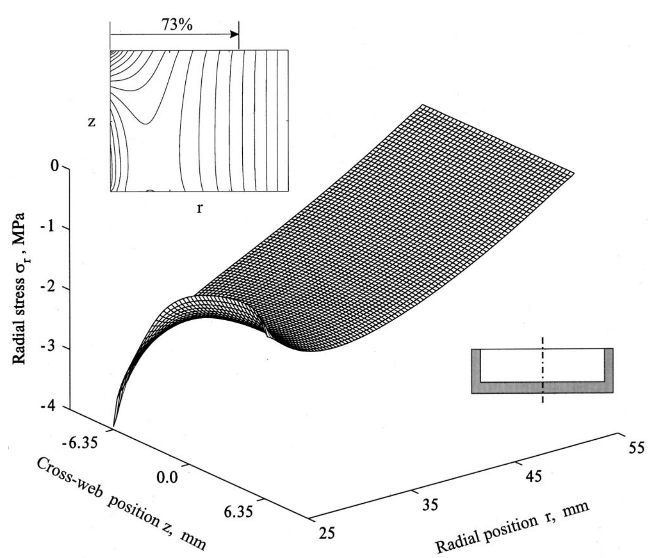

Fig. 10 Surface and contour representations of the radial and cross-web variation of σ_r; *NR*=100, *NZ*=80. The parameter values are as specified in Table 1 (plastic, cup-shaped core).

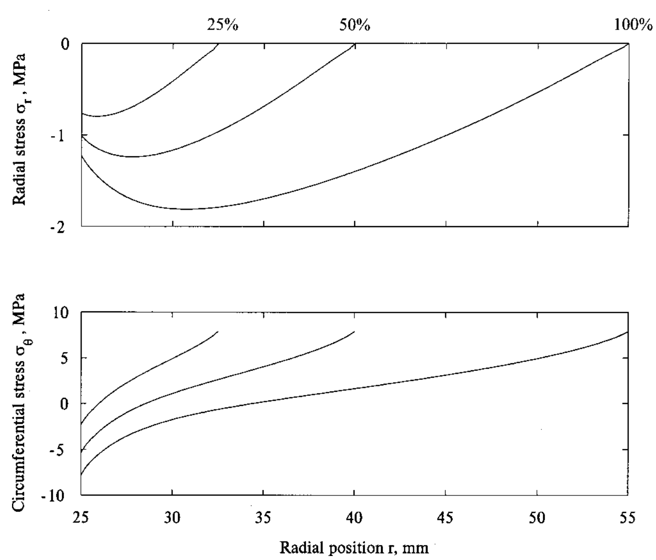

Fig. 12 Variations of σ_r and σ_θ along the roll's centerline with increasing numbers of web layers: 25 percent, 50 percent, and 100 percent of a full roll; *NR*=100, *NZ*=80. The parameter values are as specified in Table 1 (plastic, cup-shaped core).

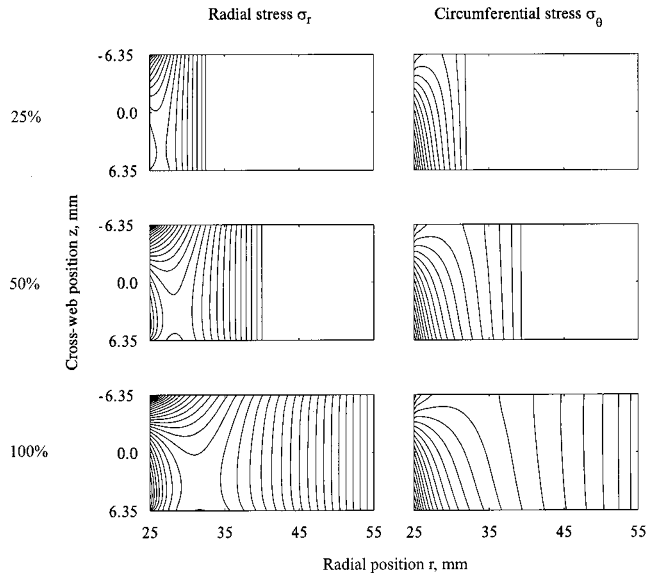

Fig. 13 Radial and cross-web variations of σ_r and σ_θ with increasing numbers of web layers: 25 percent, 50 percent, and 100 percent of a full roll; $NR=100$, $NZ=80$. The parameter values are as specified in Table 1 (plastic, cup-shaped core).

3.95 MPa at the closed stiff end to 0.89 MPa near the open compliant side. Although the gradient for σ_r near the stiff edge is steep, the solution has converged to three significant digits. The circumferential stress varies along the core-web interface from 3.92 MPa (tension) at the closed end to 15.2 MPa (compression) at the core's compliant side. Cross-web variations of σ_r and σ_θ for this geometry are more significant than for the hollow cylindrical core, and because σ_θ is not always compressive along the core-web interface, winding defects could potentially be generated in $\mathcal{W}$ on only one face of the roll.

In the region $r=25\sim40$ mm, cross-width variation of σ_r is greater than ten percent, and the cross-width variation for the radial and circumferential stresses is greater than five percent over some 73 percent and 67 percent of the roll, respectively. Contours of σ_r and σ_θ are shown as insets in Figs. 10 and 11. In this example, the stress gradients in z near the core are sufficiently large that the stress field would not be well approximated by a one-dimensional model imposing uniform width-wise core stiffness.

4.3 Variable Roll Radius. Since the stress field in a wound roll depends on the overall number of layers in the roll, Fig. 12 depicts a comparison of σ_r and σ_θ along the centerline for different numbers of wound-on layers, corresponding to quarter-full, half-full, and full rolls on a cup-shaped core. Similarly, Fig. 13 shows contour representations of σ_r and σ_θ for these cases. The compressive radial and circumferential stresses each grow as NL increases. The compressive radial stress is maximized at P2 (closed stiff end) along the core-web interface and becomes more compressive with increasing NL. The cross-web variation for the radial stress is greater than five percent over more than 70 percent of the web region for each of the three rolls.

In terms of σ_θ, the cross-web variation for the quarter and half-full rolls exceeds 26 percent and six percent, respectively, over the entire roll, excluding the outermost layer at which the boundary condition of specified tension is applied. For quarter-full, half-full, and full rolls, the σ_r values along the core-web interface are $(-1.87, -3.01, -3.95)$ MPa at the closed end; $(-0.76, -1.00, -1.21)$ MPa at the centerline; and $(-0.77, -1.05, -1.20)$ MPa at the open end. Likewise, the σ_θ values at those points are (6.20, 5.01, 3.92) MPa, $(-2.37, -5.47, -8.03)$ MPa, and $(-7.94, -12.12, -15.21)$ MPa, demonstrating the presence of significant cross-width variation. In each case, σ_θ varies further from tension to compression across the roll's width.

5 Summary

The width-wise variation of stresses in wound rolls is investigated by using a two-dimensional, axisymmetric, finite element model. The present analysis relaxes assumptions made in previous one-dimensional models in which the roll was specified to be infinitely wide and with uniform core stiffness, winding tension, and material properties. By separating the wound roll into two regions—the core and layered web substructures—general core geometry and designs can be accommodated, analyzed, and optimized.

In several case studies with different materials and core geometry, the radial and cross-web variations of the σ_r, σ_θ, σ_z, and σ_{rz} stress components, as well as stress concentration or potential singularity at the free edges of the core-web interface, are investigated. The transverse and shear stress in these examples are significant only near the core-web interface and are attributed to Poisson coupling and strain mismatch between material properties. The model can be used for quantifying stress concentration at edges of the core-web interface, and for identifying material combinations and core designs for which certain stress components are expected to be finite or singular. The model can further be applied to investigate the stress state in the presence of nonuniform winding tension or material thickness across the web's width, and those areas are subjects of current investigation.

Acknowledgment

This work was supported in part by Imation Corporation and the National Science Foundation.

References

[1] Altmann, H. C., 1968, "Formulas for Computing the Stresses in Center-Wound Rolls," J Tech. Assoc. Paper Pulp Indust., **51**, pp. 176–179.

[2] Tramposch, H., 1965, "Relaxation of Internal Forces in a Wound Reel of Magnetic Tape," ASME J. Appl. Mech., **32**, pp. 865–873.

[3] Tramposch, H., 1967, "Anisotropic Relaxation of Internal Forces in a Wound Reel of Magnetic Tape," ASME J. Appl. Mech., **34**, pp. 888–894.

[4] Yagoda, H. P., 1980, "Resolution of a Core Problem in Wound Rolls," ASME J. Appl. Mech., **47**, pp. 847–854.

[5] Connolly, D., and Winarski, D. J., 1984, "Stress Analysis of Wound Magnetic Tape," *ASLE Tribology and Mechanics of Magnetic Storage Media*, Special Publication 16, ASLE, pp. 172–182.

[6] Pfeiffer, J. D., 1979, "Prediction of Roll Defects from Roll Structure Formula," J. Tech. Assoc. Paper Pulp Indust., **62**, pp. 83–88.

[7] Hakiel, Z., 1987, "Nonlinear Model for Wound Roll Stresses," J. Tech. Assoc. Paper Pulp Indust., **70**, pp. 113–117.

[8] Willett, M. S., and Poesch, W. L., 1988, "Determining the Stress Distributions in Wound Reels of Magnetic Tape Using a Nonlinear Finite-Difference Approach," ASME J. Appl. Mech., **55**, pp. 365–371.

[9] Bourgin, P., and Bouquerel, F., 1993, "Winding Flexible Media: A Global Approach," Adv. Inf. Storage Syst., **5**, pp. 493–512.

[10] Keshavan, M. B., and Wickert, J. A., 1997, "Air Entrainment During Steady State Web Winding," ASME J. Appl. Mech., **64**, pp. 916–922.

[11] Good, J. K., Pfeiffer, J. D., and Giachetto, R. M., 1992, "Losses in Wound-on Tension in the Centerwinding of Wound Rolls," *Web Handling*, ASME AMD-149, ASME, New York, pp. 1–12.

[12] Zabaras, N., Liu, S., Koppuzha, J., and Donaldson, E., 1994, "A Hypoelastic Model for Computing the Stresses in Center-Wound Rolls of Magnetic Tape," ASME J. Appl. Mech., **61**, pp. 290–295.

[13] Qualls, W. R., and Good, J. K., 1997, "An Orthotropic Viscoelastic Winding Model Including a Nonlinear Radial Stiffness," ASME J. Appl. Mech., **64**, pp. 201–208.

[14] Benson, R. C., 1995, "A Nonlinear Wound Roll Model Allowing for Large Deformation," ASME J. Appl. Mech., **62**, pp. 853–859.

[15] Hakiel, Z., 1992, "On the Effect of Width Direction Thickness Variations in Wound Rolls," Second International Conference on Web Handling, Oklahoma State University, pp. 79–98.

[16] Kedl, D. M., 1992, "Using a Two Dimensional Winding Model to Predict Wound Roll Stresses That Occur due to Circumferential Steps in Core Diameter or to Cross-Web Caliper Variation," Second International Conference on Web Handling, Oklahoma State University, pp. 99–112.

[17] Cole, A., and Hakiel, Z., 1992, "A Nonlinear Wound Roll Stress Model Accounting for Widthwise Web Thickness Nonuniformities," *Web Handling*, ASME AMD-149, ASME, New York, pp. 13–24.

[18] Zienkiewicz, O. C., and Taylor, R. L., 1989, *The Finite Element Method*, Vols. 1 and 2, McGraw-Hill, New York.
[19] Bogy, D. B., 1970, ''On the Problem of Edge-Bonded Elastic Quarter-Planes Loaded at the Boundary,'' Int. J. Solids Struct., **6**, pp. 1287–1313.
[20] Folias, E. S., 1989, ''On the Stress Singularities at the Intersection of a Cylindrical Inclusion With the Free Surface of a Plate,'' Int. J. Fract., **39**, pp. 25–34.
[21] Dundurs, J., 1967, ''Effect of Elastic Constants on Stress in a Composite Under Plane Deformation,'' J. Compos. Mater., **1**, pp. 310–322.
[22] Wang, S. S., and Choi, I., 1982, ''Boundary Layer Effects in Composite Laminates: Part I—Free-Edge Stress Singularities,'' ASME J. Appl. Mech., **49**, pp. 541–548.
[23] Wang, S. S., and Choi, I., 1982, ''Boundary Layer Effects in Composite Laminates: Part II—Free-Edge Stress Solutions and Basis Characteristics,'' ASME J. Appl. Mech., **49**, pp. 549–560.
[24] Tsamasphyros, G., 1987, ''Methods for Combination of Finite Element and Singular Integral Equation Methods,'' Comput. Methods Appl. Mech. Eng., **60**, pp. 45–56.